



**HAL**  
open science

# Evolution of particle interactions between accidentally released aerosol particles generated from powdered engineered nanomaterials into a simulated workplace atmosphere

Georgios F. Kylafis, Alison S. Tomlin, P. Andrew Sleight, Alexis Vignes

## ► To cite this version:

Georgios F. Kylafis, Alison S. Tomlin, P. Andrew Sleight, Alexis Vignes. Evolution of particle interactions between accidentally released aerosol particles generated from powdered engineered nanomaterials into a simulated workplace atmosphere. *Journal of Aerosol Science*, 2019, 129, pp.98-115. 10.1016/j.jaerosci.2018.12.008 . ineris-03319045

**HAL Id: ineris-03319045**

**<https://ineris.hal.science/ineris-03319045>**

Submitted on 11 Aug 2021

**HAL** is a multi-disciplinary open access archive for the deposit and dissemination of scientific research documents, whether they are published or not. The documents may come from teaching and research institutions in France or abroad, or from public or private research centers.

L'archive ouverte pluridisciplinaire **HAL**, est destinée au dépôt et à la diffusion de documents scientifiques de niveau recherche, publiés ou non, émanant des établissements d'enseignement et de recherche français ou étrangers, des laboratoires publics ou privés.

Evolution of particle interactions between accidentally released aerosol particles generated from powdered engineered nanomaterials into a simulated workplace atmosphere.

Georgios Kylafis<sup>a</sup>, Alison S. Tomlin<sup>a</sup>, P. Andrew Sleight<sup>b</sup>, Alexis Vignes<sup>c</sup>

<sup>a</sup> School of Chemical and Process Engineering, University of Leeds , LS2 9JT, UK

<sup>b</sup> Institute of Public Health and Environmental Engineering (iPHEE), School of Civil Engineering, University of Leeds, LS2 9JT, UK

<sup>c</sup> INERIS, Parc Technologique ALATA, B.P. 2, F-60550 Verneuil-en-Halatte, France

**Keywords:** Engineered nanomaterials; exposure chamber; air quality; aerosol dynamic model

### **Abstract**

The evaluation of aerosol processes which alter the size distribution of accidentally released nanomaterial particles in an indoor environment can provide size resolved exposure estimations, and subsequently contribute to a more comprehensive risk analysis on engineered nanomaterials (ENMs). In this work processed suspensions of TiO<sub>2</sub> and SiO<sub>2</sub> nanopowders were introduced into the reservoir of a nebuliser, and injected continuously as nano-aerosols into a room-size dispersion facility for a fixed release time. Following injection, the concentration of the dispersed aerosols was allowed to naturally decay for a prolonged period. Airborne particle number concentration (PNC) and particle size distributions (PSD) were continuously measured at a point within the breathing zone near to the source, while deposited particles were collected for transmission electron microscopy (TEM) analysis. A log<sub>10</sub>-normal fitting program was used to determine the evolution of the modal groups present within the measured PSDs. A modeling approach that considered the experimentally determined particle decay rate as a sum of the pair to pair coagulation and deposition rates was employed to estimate the relative importance of size-resolved deposition compared to coagulation. Results indicated that the variation of PNC with time was accurately modelled, providing size-dependent insights into the contribution of the two particle removal mechanisms to the change of PNC over time. The deposition patterns obtained from the TEM images qualitatively supported the model results. Since a limited set of input parameters were used, we concluded that the proposed model could be an effective tool for a reasonable quantification of

worker's exposure to aerosols originating from the accidental release of diffuse ENM in real workplaces.

## **1. Introduction**

Nanotechnology is recognised as one of the most important technologies of the 21st century. However, evidence on the health (Kermanizadeh et al., 2016; Oberdörster et al., 2015; Pattan and Kaul, 2014) and environmental (Gardea-Torresdey et al., 2014; Gottschalk et al., 2013; Klaine et al., 2012) impacts caused by the use of applications and products embedding engineered nanomaterials (ENMs), have raised some concerns within the global community. The potential for human exposure to ENMs has so far been addressed to a limited degree (Nazarenko et al., 2012), and the relevant detailed information in the existing literature on exposure is often insufficient (Ding et al., 2017). To establish appropriate schemes of risk management at nanotechnology workplaces where accidental emissions of ENMs and worker population co-exist, a combination of toxicological and exposure related data should be established.

Processes at nanotechnology workplaces, such as production, transfer, packaging, transfer and processing, where high amounts of ENMs are involved, raise significant concerns regarding their safety profile. ENMs in the form of powders present a high potential for accidental dispersion (Kuhlbusch et al., 2011) leading to inhalation and to dermal exposure. Inhalation is considered as the most likely and direct route of exposure to ENMs (Methner et al., 2010a; Methner et al., 2010b), however dermal penetration or ingestion may also unintentionally occur (Brouwer et al., 2016; Filon et al., 2015). In a recent review conducted by Koivisto et al. (2017), 374 different scenarios related to nanomaterial-based products were included, and the authors concluded that the type of released particles can vary from consisting of pure nanomaterials to fully matrix embedded-nanomaterials, depending on the products and processes. Furthermore, they indicated that a well described and harmonized methodology for the exposure assessment to ENMs, should unambiguously link test procedures to data reporting, including quantification of the amount of nanomaterials released when possible.

Generated airborne nano-objects could enter the respiratory system as individual nanoparticles, nanoparticle agglomerates and nanoparticles within or attached to

larger particles (Nazarenko et al., 2012). Although a range of submicron particles ( $< 1 \mu\text{m}$ ) can effectively access the region of the alveolar where removal mechanisms are possibly insufficient (Muhlfeld et al., 2008), nanoparticles ( $< 100 \text{ nm}$ ) due to their small size, are able to pass into the deeper lung region. The deeper a particle is deposited, the longer it takes to be removed from the lung, resulting in the higher probability of adverse health effects because of particle-tissue and particle-cell interactions (Blank et al., 2009).

There are three main metrics used within exposure assessments for airborne nanomaterial particles. These are: i) mass concentration ( $\text{mg}\cdot\text{m}^{-3}$ ); ii) number concentration ( $\text{n}\cdot\text{m}^{-3}$ ) and; iii) surface area concentration ( $\text{m}^2\cdot\text{m}^{-3}$ ). Instrumentation is available to measure each of these metrics. There is a growing body of discussion related to the metrics used in the establishment of occupational exposure limits for ENMs. According to Delmaar et al. (2015), at a universal level, a simple dose metric for nanoparticles is still lacking. However, a combination of information about particle numbers and size distributions provides additional information compared to simple number or mass based metrics.

An important question when assessing the possible risks in accidental dispersions of ENMs is to identify and quantify the aerosol transport processes driving changes in the morphological characteristics, such as the particle size of the released nanomaterial particles, from a source to the receptor (John et al., 2017). Particle deposition and coagulation, are considered as two major mechanisms to describe the overall particle dynamics in an enclosed aerosol system (Wang et al., 2017). These two processes have been studied by many groups as a function of the particle size distribution (PSD) and the particle number concentration (PNC) (Jamriska and Morawska, 2003; Maynard and Zimmer, 2003; Schnell et al., 2006). They concluded that for the establishment of indoor air quality (IAQ) models, information such as deposition rates and coagulation coefficients, are required.

Surface deposition will come into play as a sink during transport from the source to the receptor and as a mechanism responsible for surface contamination (Schneider et al., 2011). The review of Lai et al. (2002) included experimental measurements of surface particle deposition velocities as obtained by various studies, and a U-shape feature of the size-resolved deposition velocity occurred. The deposition process of ultrafine particles ( $<0.1 \mu\text{m}$ ) is considered to be affected by Brownian and turbulent

diffusion, whereas gravitational settling is more important for particles larger than 1  $\mu\text{m}$ . Finally, for those particles between 0.1-1  $\mu\text{m}$ , the dominant mechanism is not quite clear.

On the other hand, extensive dynamic analysis on size-resolved measurements of indoor aerosols in real buildings has been conducted by several studies in order to track the effect of coagulation on the PNC decay following an episodic release (Rim et al., 2012; Wallace et al., 2008; Yu et al., 2013). These studies indicated that particle coagulation as a removal process for the ultrafine particles is enhanced by higher PNC due to the higher probability for interparticle collisions compared with the larger ones, where factors such as the particle size, Brownian motion, Van Der Waals force, viscosity and aggregate state have been considered to affect the coagulation.

Several facilities have been utilised for the study and validation of indoor settings dealing with the release of aerosols originating from specific ENMs (Seipenbusch et al., 2008; Walser et al., 2012; Wang et al., 2017). The importance of the background particle concentration or large associated particles in the fate and behaviour of the smaller particles has been highlighted. Furthermore, it has been confirmed that dispersed nanomaterial particles are subjected to mechanisms that modify their morphological characteristics throughout their transportation from the emission source to the receptor. Considering the polydisperse particle size nature of nanopowders, it is expected that in the case of an accidental dispersion, large airborne nanoparticle agglomerates would be released, demonstrating scavenging activity over the smaller particles.

Currently, a widely used approach considers that if coagulation is negligible, the decay of an instantaneously released aerosol into a well-mixed and air-tight enclosure can be described in a discrete form as:

$$N(d_i, t) = N_{d_{i,0}} \exp(-\beta_{d_i} t) \quad (1)$$

where  $N(d_i, t)$  is the concentration of particles with diameter  $d_i$  at time  $t$ ,  $\beta_{d_i}$  is the size-dependent particle decay rate,  $t$  is the elapsed time, and  $N_{d_{i,0}}$  is the initial indoor concentration of particles with diameter  $d_i$ . Eq. (1) has been used by many researchers to analytically describe and quantify particle deposition by mass or number in indoor environments or experimental chambers, through the experimentally based

determination of  $\beta_{d_i}$  (He et al., 2005; Hussein et al., 2009; Lai and Nazaroff, 2005; Lai, 2006; Lai et al., 2002; Thatcher et al., 2002).

Plots of the logarithmic values of  $N(d_i, t)$  versus time corresponding to the decay period enable the calculation of  $\beta_{d_i}$  through the gradient of the best fitted line. Yu et al. (2013) established a universal criterion to evaluate whether coagulation can be ignored relative to deposition for a specific aerosol through the assessment of the ratio of coagulation to deposition, combining both experimental and theoretical work. They concluded that within the ultrafine size range the ratio of coagulation to deposition becomes more and more significant with increasing particle size, but it is inversed in the  $\mu\text{m}$  size range. However, the evaluation of whether coagulation can in fact be ignored relative to deposition within the losses represented by the particle decay rate  $\beta_{d_i}$ , is still lacking investigation. Furthermore, this assumption should be investigated in relation to particle size effects through a size-resolved analysis over the entire range of the size distribution of an aerosol.

The development of simplified models, with reduced input parameters, whilst still representing the important particle processes, coupled with their validation through experimental measurements, would help to provide tools that may be used to estimate the potential exposure to accidentally released nanomaterial particles in the workplace with reduced on-site measurements. In this work, the term “accidentally” has been used to describe a high energy input to a powdered ENM, such as a leak in a pressurised vessel that may lead to a significant high release of nanomaterial particles and subsequently to high exposure levels in a confined environment without mechanical ventilation (worst case scenario).

In order to investigate and validate the above assumption, liquid atomisation was applied in order to disperse nanomaterial particles originating from specific powdered ENMs into a dispersion chamber of a scale representative of a typical workplace, for a fixed release time. The evolution of the PSD and the size-resolved PNC during the release period, and a subsequent prolonged decay period, was tracked by real-time measurement devices operating in parallel near to the source and within the human breathing zone (1.50 cm above ground, see Fig. 1b below). The choice of instrumentation covered both the nano and micron scale, providing the basis for the deduction of the governing kinetics. A  $\log_{10}$ - normal fitting program was used to

distinguish the different modal groups within the measured PSD, thus highlighting the interactions of the released aerosol particles over time. Deposited particles were collected for transmission electron microscopy (TEM) analysis.

A particle dynamic model was developed to investigate the differential effect of coagulation and deposition on the changes in PNC with time for both experimental periods. The modelled coagulation sinks, and the experimentally determined total particle loss sinks, were used to estimate the deposition sinks through the assumption that the particle decay rate  $\beta_{d_i}$  represents both coagulation and deposition losses. The modelled source rates provided estimates for modelling purposes relating to the injection stage. All the above were introduced into a size-resolved equation predicting the time-dependent changes in PNC of specific diameter particles within what is considered to be a well-mixed chamber. The estimated changes in PNC were then compared with the experimental measurements and served to highlight the importance of the different physical experimental processes in the change of exposure to particles within different size ranges during and after the indoor accidental release of nanomaterial particles.

## **2. Material and methods**

### **2.1 Experimental set-up**

The experimental chamber used for the study is of volume 32 m<sup>3</sup> and is constructed from prefabricated, plastic coated, wipe clean panels. There are two air inlets into the main test chamber, one located at a low level on the left hand wall, and the other located in the ceiling. Air entering the test chamber is taken from outside the building through a pipe network and is HEPA filtered before being conditioned by a humidifier and heater, establishing a well-controlled environment to correctly interpret the acquired experimental data. One inlet and one outlet mounted on the wall were used for sampling and for the introduction of aerosols into the chamber. Shut-off dampers were present in both the inlet and outlet in order to ensure the internal volume was isolated during the release tests and the prolonged period following the end of release. Further details regarding the dispersion chamber are provided elsewhere (Kylafis, 2016).

A fan at the bottom of the chamber was operating during the entire experimental period (aerosol injection and the following decay period) in order to establish good

mixing conditions within the chamber. No extra treatment was applied for the inner surface and the shell of the chamber to minimise the deposition of aerosol particles. The temperature and relative humidity (RH) of the chamber were monitored during the experiments via a Tinytag Ultra 2 TGU-4500 data logger, installed at the sampling point A. The scheme of the experimental set-up is shown in Fig. 1.

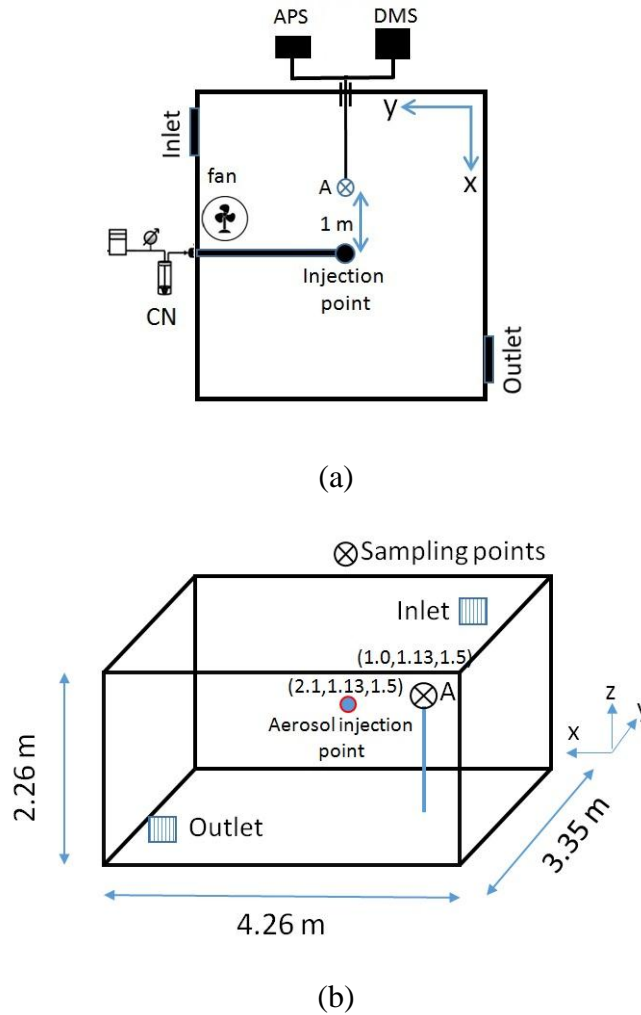


**Fig. 1:** (a) Main test chamber dimensions, with air inlet and outlet locations; (b) floor plan of the main chamber indicating the location of the experimental measurement devices

## 2.2 Aerosol generation

Polydisperse  $\text{TiO}_2$  and  $\text{SiO}_2$  aerosols were generated via an injection system consisting of a 6-jet Collison Nebuliser (CN, BGI Inc., USA), a stainless steel tube of 1.13 m length and 2.7 cm ID, a separate pump, pressure regulator and meter operating at a flow rate of  $8 \text{ l min}^{-1}$  to deliver HEPA filtered air for the carrier gas. The tube was operating as a drying section by wrapping it in a heated tape at  $50 \text{ }^\circ\text{C}$  to enhance the

removal of humidity from the produced aerosol before its dispersion in the room. The colloidal suspensions were prepared by dispersing given amounts (1.5 g) of Aeroxide TiO<sub>2</sub> P25 (Evonik industries, Essen, Germany) (average primary particle size 21 nm and specific surface area  $50 \pm 15 \text{ m}^2/\text{g}$ ) and Synthetic Amorphous SiO<sub>2</sub> (NM-200) (provided by the Joint Research Centre, Ispra, Italy) (average primary particle size  $14 \pm 7 \text{ nm}$  and specific surface area  $189.2 \text{ m}^2/\text{g}$ ) nanopowders into Type I biological grade de-ionised water ( $\geq 18 \text{ M}\Omega\text{cm}$  resistivity) by an ultrasonic probe.

These processes enabled the production of nano-suspensions characterised by multimodal size distributions and by the presence of particles with diameter  $\leq 100 \text{ nm}$ ; the latter was not seen in the case of their respective unprocessed suspensions. At the same time, this method resulted in the elimination of the presence of particles in the micron scale and in the establishment of electrical stability based on pH measurements in the produced suspensions. The fragmentation occurring in suspensions of both tested materials after undergoing sonication can be seen in Fig. A1 (Appendix A), where the averaged volume-based distributions as measured by the dynamic light scattering (DLS) technique over three sonicated and three unsonicated samples (suspension phase), are illustrated.

### **2.3 Measurement scenario**

Before each measurement, the chamber was rinsed with ultra-pure water, wiped with dust-free paper and ventilated at 12 air changes per hour (ACH) via the ventilation control module in order to obtain a particle-free environment (background PNC  $< 800 \text{ cm}^{-3}$ ). Aerosol particles were then continuously injected into the chamber through the inlet at a well-controlled flow rate. At the same time, the measurement devices presented below began the monitoring process. When the aerosol particles reached the desired number concentration (sufficient to accurately measure the concentration decay in the chamber), the 6-jet CN was stopped. In the subsequent, post release period, the dispersed aerosol was allowed to naturally decay for 5 hours, under unventilated conditions. Three replicate tests were conducted for each of the tested materials. Inlet temperature was relatively constant throughout the experiments ( $22.66 \pm 1 \text{ }^\circ\text{C}$ ). The relative humidity was  $56 \pm 4 \text{ \% RH}$  and  $61 \pm 6 \text{ \% RH}$ , throughout the injection and decay period, respectively. According to Wang et al. (2017), these RH levels are considered as normal without a significant impact on the particle deposition rates.

A differential mobility spectrometer (DMS500 by Cambustion Ltd, UK) and an aerodynamic particle sizer (APS model 3321, TSI Inc, USA) located at a specific access port outside the wall of the dispersion facility, were employed for simultaneous monitoring of the PSD at position A, as indicated in Fig. 1. Also shown are the coordinates of the sampling point, as well as those of the aerosol injection point. The DMS allowed measurement of PSD within the diameter range 5-1000 nm based on the particle mobility within an electric field, whereas the APS measured PSD based on the light scattering intensity in the equivalent optical size range of 0.5-20  $\mu\text{m}$ . The aspiration rate of the DMS was 8 l/min and that of the APS was 1 l/min.

External silicone conductive tubing (1 m long and 1/4" ID) was used for sampling the indoor air through an access port of the chamber, as shown in Fig.1. The PSD were measured in the near field, at a 1 m distance from the source and at a height of 1.50 m. Since two measurement devices were sampling in parallel at position A, the aerosol stream was split into two via a Y connector fitted through the wall of the chamber.

Metallic stubs were placed at various locations on the floor and the walls of the chamber in order to collect deposited matter for subsequent TEM analysis. Specifically, 400 mesh Cu grids coated with holey carbon film (Agar Scientific) were attached to standard Al SEM stubs (Agar Scientific) using a spot of silver dag. Once the grids were attached, the stubs were placed inside the process chamber at various locations on the floor and the walls so particles could attach to the grids. After the experiments the grids were carefully removed from the stubs using tweezers and then transferred to the TEM for examination. The TEM used was an FEI Tecnai TF20 of high resolution suitable for cryo-electron microscopy single particle specimens and semi-thick frozen cells (or sections up to 200 nm).

The diffusion loss for particles larger than 20 nm within the transportation tubing computed by the particle loss calculator software tool (Von der Weiden et al., 2009) was less than 3.5 % for the combined flow rate (9 l/min) of the aerosol stream starting from position A, where the DMS and APS were simultaneously sampling. Therefore, we did not implement additional corrections related to the transportation tubing. Additionally, the effect of siloxane degassing from the transportation tubing may have altered the gas composition of the sample aerosol with subsequent effects on the charging efficiency of the unipolar diffusion charger utilised by the DMS, as indicated in the work of Asbach et al. (2016). However, due to the high flow rate of aerosol

sampled from position A, the concentration of emitted gas can be considered as low, reducing any potential effect on aerosol particles, as well as on subsequent sampling.

The number based PSDs from the DMS and APS, are presented as  $dN/d\log(d_p)$  (relative number concentration), where  $dN$  is the number of particles detected in a size channel, and  $d\log(d_p)$  is the difference between the logarithms of the upper and the lower channel diameters. As indicated above, the DMS and APS measure electrical mobility and aerodynamic diameters, respectively. By assuming that particles are spherical and of  $1 \text{ g/cm}^3$  density, then the two diameters could be considered as comparable (Nazarenko et al., 2012). Therefore, the data obtained from the two measurement devices was interpreted as measurements on the same particle-size scale.

## **2.4 Data analysis**

### **2.4.1 Modal parameter fitting procedure**

The PSDs measured by the DMS were modelled in order to study the evolution of the component modes over time. PSDs from monodisperse sources are well known to be mathematically described by  $\log_{10}$ -normal distributions. Since the present work studies airborne aerosol particles originating from nanopowders, their diameters are expected to range over several orders of magnitude. Therefore, as indicated by various other outdoor atmospheric studies (Agus et al., 2007; Lingard et al., 2006; Whitby, 1978), this wide range of particle diameters results in a better description of the PSD by using a sum of  $\log_{10}$ -normal size distributions described by a small number of parameters.

In this work, a modal fitting program, Rmixdist, was used to estimate the modal PNC (mPNC), count median diameter (CMD) and geometric standard deviation ( $\sigma_g$ ) of the modes within the measured PSDs. A full description of the program is provided by (Leys et al., 2005). Indicatively, based on the aerodynamic processes governing atmospheric aerosols, Schneider et al. (2011) utilised the following size ranges to characterise the PSDs of aerosols at workplaces: nucleation mode ( $< 25 \text{ nm}$ ), Aitken mode ( $25 - 100 \text{ nm}$ ) which is the transition mode between nucleation and accumulation modes, accumulation mode ( $100 - 1000 \text{ nm}$ ), and coarse mode ( $> 1000 \text{ nm}$ ).

In this work, three modes were initially fitted to the PSD, with the number of modes fitted increased until the modelled PSD accurately described the experimental PSD. As a result, the PSDs measured within this study consisted of five to seven modes, depending upon the material and the associated emission profile, and thus it was possible for more than one mode to exist within the categories defined by Schneider et al. (2011).. An example of a campaign averaged PSD over a 10 min interval during the injection of TiO<sub>2</sub> into the dispersion chamber, along with the log<sub>10</sub>-normal component modes fitted by Rmixdist, is shown in Fig. B1 (Appendix B).

#### 2.4.2 Analytical model

According to Schneider et al. (2011), for a completely (and instantly) mixed room, the time dependent change of PNC with diameter  $d_i$ ,  $N(d_i, t)$ , in the room can be described by:

$$\frac{\Delta N(d_i, t)}{\Delta t} = \frac{S(d_i, t)}{V} + \left(\frac{\Delta N(d_i, t)}{\Delta t}\right)_{coag} + \left(\frac{\Delta N(d_i, t)}{\Delta t}\right)_{loss} \quad (2)$$

where  $S(d_i, t)$  is the source rate (particles/s) of the dispersed nanomaterial particles with diameter  $d_i$  in the room and  $V$  is the volume of the room. The subscripts “*coag*” and “*loss*” refer to changes due to coagulation and surface deposition-ventilation respectively. Since the experiments were conducted without ventilation, the last term of the right hand part of the above equation refers exclusively to deposition. It should be noted that the particle losses imposed by the measurement devices due to sampling were considered to not significantly affect the coagulation and deposition processes, therefore these were ignored in the calculations.

The source rate  $S(d_i, t)$  of particles with diameter  $d_i$  was calculated from the formula found in the work of Wallace et al. (2004):

$$S(d_i, t) = \frac{V\beta_{d_i}(N(d_i, t) - N_{d_i(0)})}{1 - \exp(-\beta_{d_i}t)} \quad (3)$$

where  $N_{d_i(0)}$  is the initial PNC of particles  $d_i$  in the testing room of volume  $V$  before the start of injection process,  $\beta_{d_i}$  is the size-dependent particle decay rate, and  $t$  is the elapsed time (s).

The change in PNC of diameter  $d_i$  due to coagulation can be expressed by the following equation (Kulmala et al., 2001; Mönkkönen et al., 2004):

$$\frac{\partial N_{d_i}}{\partial t} = J_{d_i} - CoagS \cdot N_{d_i} \quad (4)$$

where  $N_{d_i}$  - number concentration particles of size  $d_i$  ( $\text{cm}^{-3}$ )  
 $J_{d_i}$  - formation rate of size  $d_i$  particles based on  
- coagulation losses ( $\text{cm}^{-3}\text{s}^{-1}$ ), and  
 $CoagS$  - coagulation sink ( $\text{s}^{-1}$ )

In this work, coagulation was determined by both self-coagulation and coagulation scavenging. The coagulation sink in a discrete form is expressed as (Kulmala et al., 2001):

$$CoagS = \sum_j K_{i,j} N_{d_j} \quad (5)$$

where  $K_{i,j}$  - coagulation coefficient between particles  $d_i$  and  
 $d_j$ ,  $j \geq i$ , ( $\text{cm}^{-3}\text{s}^{-1}$ ), and  
 $N_{d_j}$  - number concentration particles of size  $d_j$  ( $\text{cm}^{-3}$ ),

The formation rate of particles  $d_i$  based on the coagulation losses ( $J_{d_i}$ ), on the right hand side of Eq. (4), in a discrete form is given by the equation (Schneider et al., 2011):

$$J_{d_i} = \frac{1}{2} \sum_j^{i-j} K_{i-j,j} N_{d_{i-j}} N_{d_j} \quad (6)$$

where  $K_{i-j,j}$  - coagulation coefficient between  
particles  $d_{i-j}$  and  $d_j$ ,  $j < i$ , ( $\text{cm}^{-3}\text{s}^{-1}$ ),  
and,  
 $N_{d_{i-j}}$  - number concentration particles of  
size  $d_{i-j}$  ( $\text{cm}^{-3}$ ).

The coagulation coefficient is found using the following equations (Kulmala et al., 2001):

$$K_{i,j} = \pi(D_i + D_j)(d_i + d_j) \times \left( \frac{d_i + d_j}{d_i + d_j + 2(g_i^2 + g_j^2)^{1/2}} + \frac{8(D_i + D_j)}{(c_i^2 + c_j^2)^{1/2}(d_i + d_j)} \right)^{-1} \quad (7)$$

where  $D_i$  and  $D_j$  are the particle diffusion coefficients ( $\text{cm}^2 \text{s}^{-1}$ ) for particles  $d_i$  and  $d_j$  respectively, given by the equations:

$$D_i = \frac{kT}{3\pi\mu d_i} \left( \frac{5 + 4Kn_i + 6Kn_i^2 + 18Kn_i^3}{5 - Kn_i + (8 + \pi)Kn_i^2} \right) \quad (8)$$

$$g_i = \frac{1}{3d_i\ell_i} \left[ (d_i + \ell_i)^3 - (d_i^2 + \ell_i^2)^{3/2} \right] - d_i \quad (9)$$

$$Kn_i = \frac{2\lambda_{air}}{d_i} \quad (10)$$

$$\ell_i = \frac{8D_i}{\pi c_i} \quad (11)$$

$$c_i = \left( \frac{8kT}{\pi m_i} \right)^{1/2} \quad (12)$$

where  $m_i$  is the mass of particle  $d_i$  (kg). The constants assumed in Eqs. (7)-(12) are:  $T = 25 \text{ }^\circ\text{C}$  or  $298 \text{ K}$ ,  $\rho = 1,0 \text{ g cm}^{-3}$ ,  $\lambda_{air} = 0.0686 \text{ } \mu\text{m}$ ,  $\mu = 1.83 \times 10^{-4} \text{ g cm}^{-1} \text{ s}^{-1}$ ,  $k=1.38 \times 10^{-23} \text{ J/K}$ , and  $K_n=$  Knudsen number.

Through Eq. (2), the changes in PNC during the determined time interval  $\Delta t$  were estimated. The injection stage was divided into 14 time intervals (5 min each), and the 5 h post release period, into 30 time intervals (10 min each). Since the DMS measurements are based on discrete particle size bins, the equation was applied separately for each bin and calculations allowed comparisons between the modelled and the averaged experimental data over the specified time intervals. Through Eq. (3), the source rates of particles of a given size were calculated based on the 1 second DMS scans and values were averaged over the  $\Delta t$  time intervals determined for Eq. (2), whereas for the decay period the source rate term was set to zero. Using Eqs. (5) - (12) the coagulation sinks for individual particles of a given size during the determined experimental periods have been calculated based on the averaged DMS measurements over the  $\Delta t$  time intervals.

As indicated in the introduction section, the factor  $\beta_{d_i}$  was considered to represent the total particle losses including both coagulation and deposition. The plots of the logarithmic values of  $N(d_i, t)$  versus time obtained by the DMS during the decay period, enabled the calculation of  $\beta_{d_i}$  through the gradient of the best fitted line with regression coefficient  $R^2 > 97\%$ . Therefore, with known total particle losses and calculated losses due to coagulation, an estimation of the deposition losses with time can be obtained during the entire experimental period, by subtracting the latter from the former.

The sinks were based on coagulation to particles  $\leq 2.5 \mu\text{m}$ , including the overall nanoscale defined by the detection ability of the DMS and the upper limit of the APS where  $\mu\text{m}$ -particles were able to be detected. It should also be noted that the particles in the micron-scale were considered to contribute to coagulation as scavengers over nanoscale particles, excluding self-coagulation (homogeneous coagulation).

### **3. Results and discussion**

#### **3.1 Experimental results**

Figs. 2 and 3 present the evolution of the average PSD over time for the  $\text{TiO}_2$  and  $\text{SiO}_2$  aerosol, respectively, as measured by the DMS and the APS. Each data point represents the channel-specific relative number concentration averaged over each ten-minute interval of the total experimental period and for all replicates of each case. Due to the extended length of the decay period, the first 10 min intervals of each hour following the end of injection and the last 10 min interval of the particular period, are presented. The inserted tables into the graph windows summarise the total PNC corresponding to the first and to the last interval of each experimental period (injection and 5 hour decay period), as measured by the DMS for particles  $\leq 1 \mu\text{m}$ , and by the APS for particles  $> 1 \mu\text{m}$  in diameter.

The standard error of the mean of the ten minute averages across the three replicates was found to vary with particle size. Specifically, the standard error in DMS measurements typically represented 5-25 % and 4-15 % of the mean number concentration value within each particle size bin, while that in APS measurements typically represented 4-9% and 3-6.5% of the mean number concentration value within each particle size bin, for the  $\text{TiO}_2$  and  $\text{SiO}_2$  dispersion tests respectively. This

difference between standard errors can be attributed to the fact that the two instruments use different principles to measure particle size, with the DMS being more vulnerable to variability due to its electrometers. The highest standard errors were observed for the smallest size bin of the DMS, since the number concentrations were low and therefore comparable to the noise level of the instrument resulting in fluctuations in measurements.

As can be seen in Figs. 2a and 3a, the subsequent PSDs during the injection stage of both tested materials, each showed a slow but stable shift of the central particle mode diameter to larger sizes. Also, it is interesting to note that in the case of SiO<sub>2</sub>, there is a strong presence of what would usually be classified as nucleation mode particles (diameter < 25 nm).

Significant decay of the total PNC can be seen within the first hour of the decay period, for both tested materials (from  $2.40 \times 10^5$  to  $1.42 \times 10^5$  #/cm<sup>3</sup>, and from  $1.65 \times 10^5$  to  $1.15 \times 10^5$  #/cm<sup>3</sup>, for TiO<sub>2</sub> and SiO<sub>2</sub>, respectively). For the SiO<sub>2</sub> decay period (Fig. 3b), a gradual shift of the dominant mode in the nanoscale to larger diameters can be seen throughout the whole study period of 5 hours. At the same time, it is shown that the PSD rapidly narrowed within the first hour of the decay period, with substantial losses of the smallest particle sizes. These losses could be attributed to high coagulation rates developed for these small particles after the termination of a constant supply of fresh aerosol by the source. In contrast to TiO<sub>2</sub>, while the main mode was located at 177 nm at the start of the decay process, it continuously increased up to 198 nm at the end of the final 10-minute interval. The drop in the total PNC within the first hour of the decay process (from  $1.65 \times 10^5$  to  $1.15 \times 10^5$  #/cm<sup>3</sup>) was more moderate compared to that observed for TiO<sub>2</sub> (from  $2.40 \times 10^5$  to  $1.42 \times 10^5$  #/cm<sup>3</sup>). This could be attributed to differences in the relative importance between particle loss mechanisms, resulting in the observed small shifts of the main mode toward to larger sizes.

On the other hand, the APS measurements indicated the presence of coarse particles (> 1 μm), described by an increasing trend during injection (Figs. 2a and 2b). However, their number concentration was substantially lower than that of submicron particles, whereas in the case of SiO<sub>2</sub>, their number concentration was substantially lower compared to those observed in the TiO<sub>2</sub> dispersion tests. Finally, during the 5

hour period following the end of injection (Figs. 2b and 3b), their PNC was shown to gradually decrease, possibly due to surface deposition induced by gravitational settling (Lai, 2002), a process that is considered to contaminate surfaces (Schneider et al., 2011).

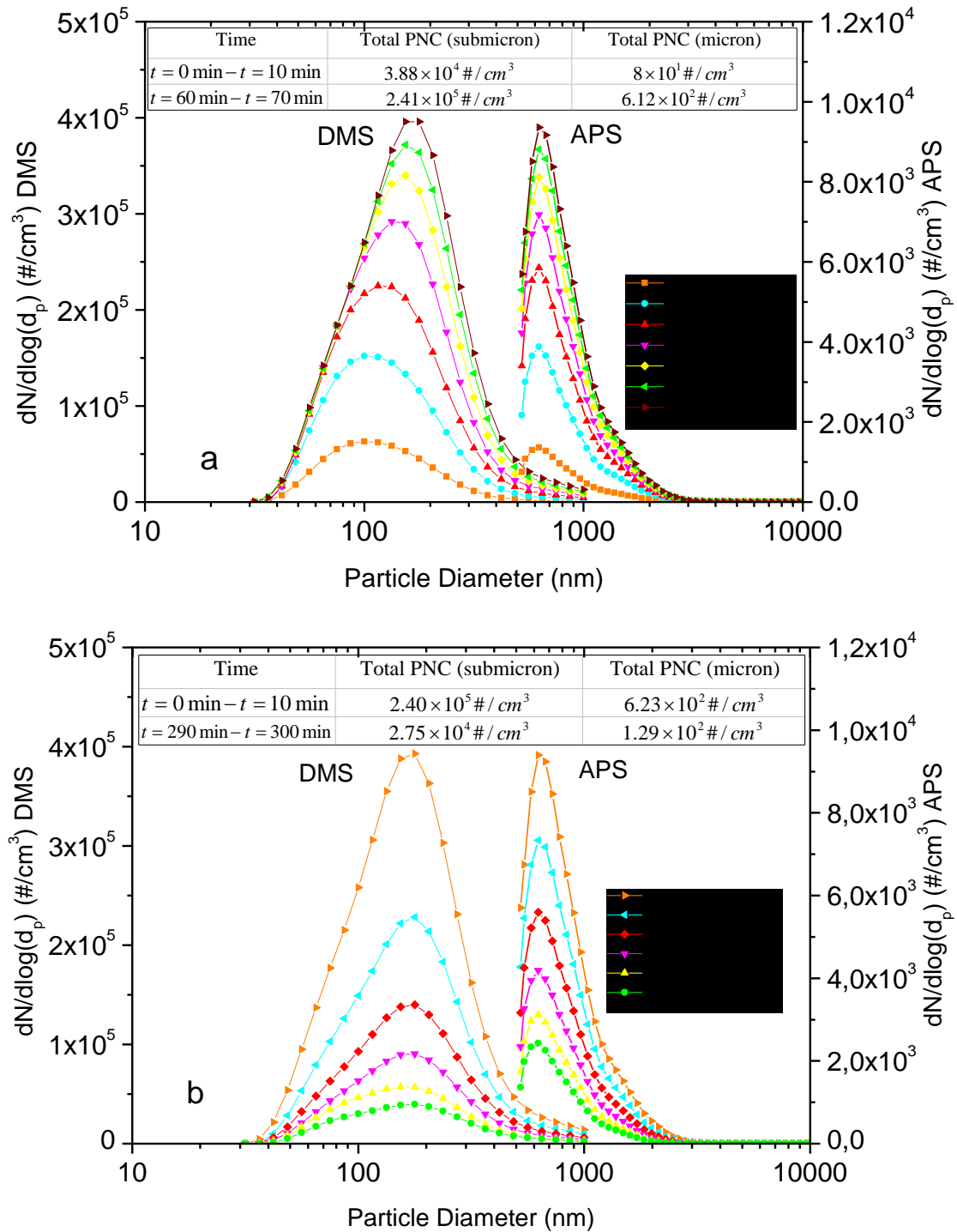


**Fig. 2:** Evolution with time of the average PSDs a) in consecutive 10 min intervals during the 70 min continuous injection period of  $\text{TiO}_2$  aerosol, and b) in the first 10 min intervals of each hour following the end of injection, up to the last 10 min

interval of the study period

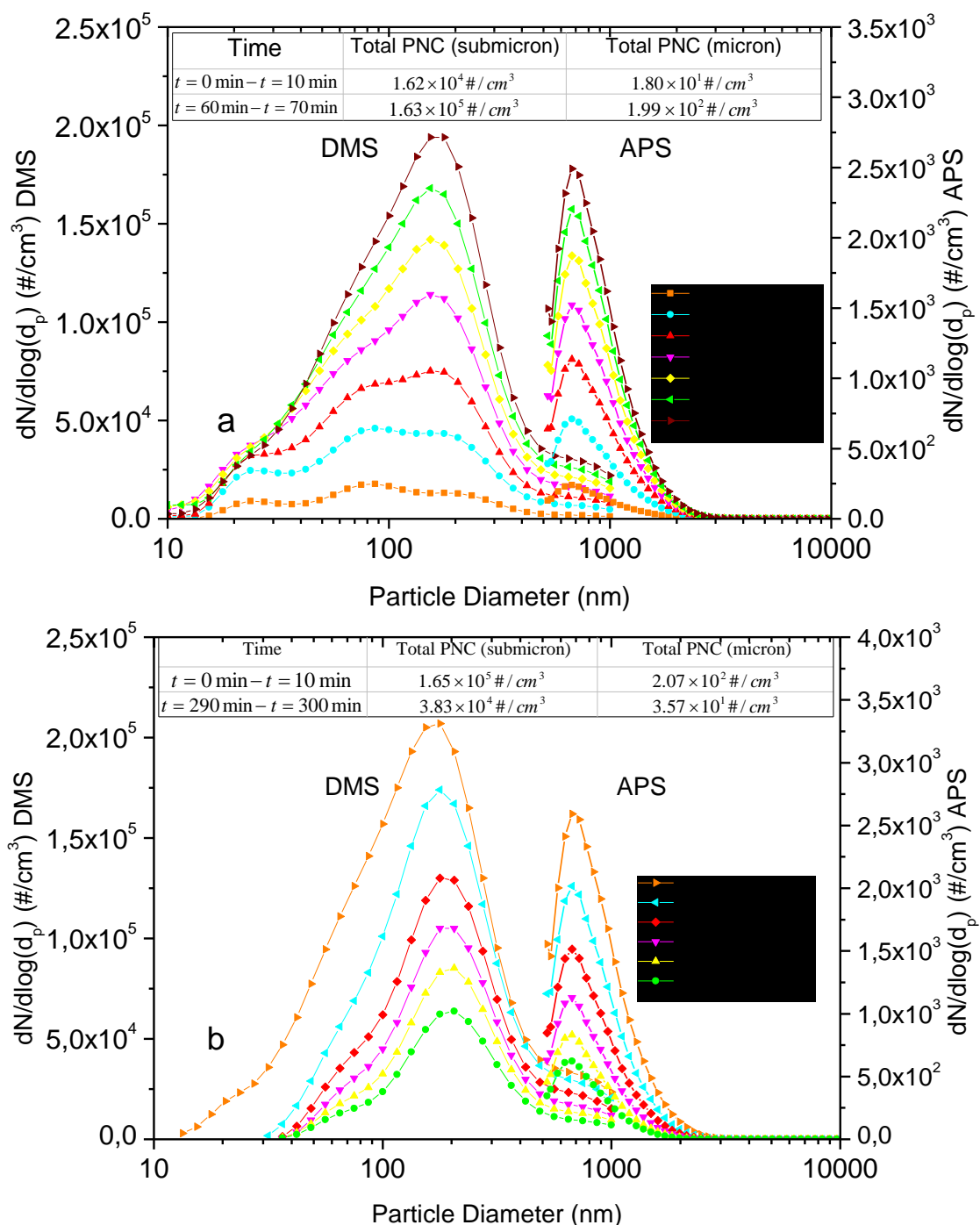


**Fig. 3:** Evolution with time of the average PSDs a) in consecutive 10 min intervals during the 70 min continuous injection period of  $\text{SiO}_2$  aerosol, and b) in the first 10 min intervals of each hour following the end of injection, up to the last 10 min interval of the study period

### 3.2 Modal fitting of particle size distributions

The average CMDs resulting from Rmixdist fitting of the PSDs measured by the DMS are shown in Fig. 4, for both tested materials and experimental periods. Based

on the atmospheric aerosol size distributions' modal characteristics, the dispersion of TiO<sub>2</sub> (Fig. 4a-b) indicates a continued presence of what would usually be classified as Aitken (25 – 100 nm) and accumulation (> 100 nm) mode particles. In addition to this, in the case of SiO<sub>2</sub> (Fig. 4c-d), the presence of modes whose diameters lie within what is usually classified as nucleation size range (0 – 25 nm) can be seen.

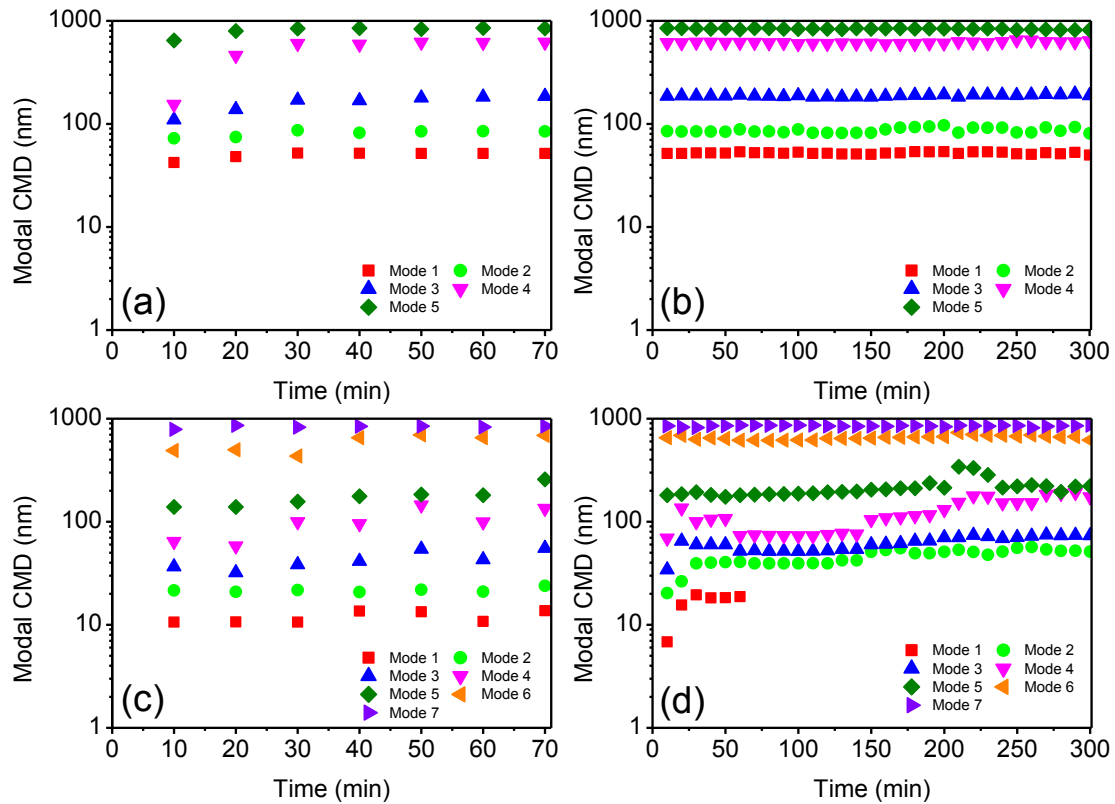


**Fig. 4:** Variations in CMDs of (a and c) the injection stage and (b and d) the 5h period following the end of injection, for (a and b) TiO<sub>2</sub> and (c and d) SiO<sub>2</sub> dispersion tests respectively.

For TiO<sub>2</sub> aerosol injection, a rapid shift of all the modes towards larger sizes at the end of the second 10 min interval of release (Fig. 4a) can be seen, especially for larger particles. Indicative of this, is the 300 nm net increase of the diameter of Mode 4 during this time. The shifts of the modal diameters towards larger sizes continued more moderately until the end of the third 10 min interval. In the remaining time up to the end of the release process, the majority of the modes remained constant, except for Modes 3 and 4. These modes demonstrated growth from 168 nm to 185 nm and from 594 nm to 620 nm, respectively. However, during the following 5 h period (Fig. 4b), the majority of CMDs remained relatively stable, except for Mode 4 which increased by 20 nm at the end, reaching a diameter of 640 nm.

For the SiO<sub>2</sub> dispersion tests, as shown in Figs. 4c and 4d, the number of fitting modes required to adequately describe the average PSDs were seven as opposed to five required for the TiO<sub>2</sub> ones. Throughout the release process, Modes 1 and 2 demonstrated relatively stable diameter characteristics. Modes 3 and 4 remained stable during the first 20 min of injection, while a similar behaviour was demonstrated by the larger particles (Mode 5 and 6). The only exception was Mode 7 which showed a growth in diameter, from 786 nm to 859 nm, during this period. In the remaining intervals up to the end of injection, a gradual growth was demonstrated by the total number of modes in the Aitken and accumulation size region.

In the 5 h period following the end of injection, the growth process continued throughout the study period for the majority of the modes (Fig. 4d), which was not observed for their TiO<sub>2</sub> counterparts. This could be attributed to the presence of nucleation mode particles in SiO<sub>2</sub> aerosol, which may have resulted in different agglomeration rates when the chamber was filled with a sufficient PNC of larger particles. Mode 1 and 2 significantly increased in diameter during the first 30 min, with Mode 2 stabilising within the Aitken region at the end of this period. The disappearance of nucleation mode particles after the first hour can be observed. In the middle of the 5-hour period, Mode 4 passed into the accumulation region due to the continued growth process. Mode 5, with the highest particle population, incrementally reached the 220 nm in diameter at the end, from the 180 nm at the beginning. Finally, the largest Modes 6 and 7 presented a stable evolution with time, without any remarkable change in their size.

### **3.3 Contribution of coagulation and deposition to the total concentration loss**

It is clear from the discussion above that the action of the two major competing processes, coagulation and deposition, demonstrated different relative intensities that affected the PSDs of the dispersed aerosols over time, and consequently any toxicological impact related to the particle size characteristics. These two mechanisms are acting simultaneously although the relative contribution of each mechanism to the total PNC changes over time.

By grouping and summing the measured PSDs from the DMS, and those estimated by the modelled changes in PNC through Eqs. (2)-(12), over ultrafine ( $\leq 100$  nm) and

fine (>100 nm) size regions, the influence of each mechanism on the change of the associated PNC over time in Figs. 5 and 6, can be seen, for TiO<sub>2</sub> and SiO<sub>2</sub> respectively. These size class boundaries were chosen on the basis of the associated adverse health effects induced by the inhalation of such particles, as indicated in the introduction section.

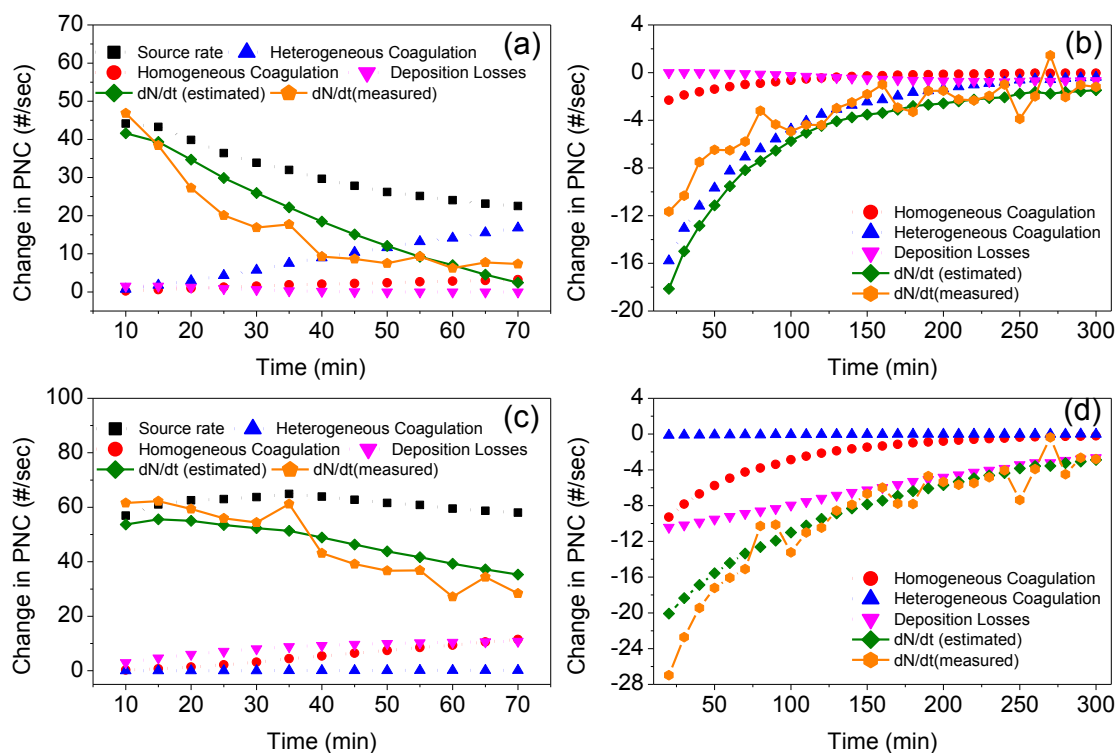


**Fig. 5:** Evolution over time of the change in PNC (estimated and measured) of TiO<sub>2</sub> aerosol due to coagulation and deposition for (a, b) ultrafine and (c, d) fine particles during the (a, c) injection stage and the (b, d) 5 h period following the end of injection.

During the early stage of the injection of TiO<sub>2</sub> aerosol, the co-existence of weak coagulation and deposition in ultrafine particles can be seen (Fig. 5a). After that period, when the chamber was filled with sufficient PNC, heterogeneous coagulation became dominant compared to deposition, resulting in the abrupt shifts of CMDs toward larger sizes at the end of the 20<sup>th</sup> minute of injection, as indicated in the modal analysis. Finally, despite the fact that the source was producing particles in the ultrafine size category, the respective calculated source rates appeared to decrease over time. Following Wallace et al. (2008), this could be attributed to the slower buildup of larger particles which are more efficient at scavenging the smaller

particles. This in turn, may results in loss rates for ultrafine size categories greater than the gain due to generation by the source.

At the same time, for fine particles the concentration decay was mainly controlled by deposition when PNC were low (see Fig. 5c); however, as PNC increased with time, homogeneous coagulation gradually increased its contribution to particle removal, leading to a balance at the end of injection when the contributions of both mechanisms became almost equal.

For the subsequent 5 h decay period under well-mixed and unventilated conditions, the dominant role of heterogeneous coagulation in the removal of ultrafine particles can be seen (Fig. 5b), demonstrating a downward trend through time, while deposition losses gradually increased, however without significant contribution to the concentration decay. When PNC became low, deposition was dominant over coagulation. On the other hand, losses of fine particles due to homogeneous coagulation exponentially decreased with time. While deposition losses also decreased throughout this period, this was at a lower rate compared to coagulation, resulting in the domination of the former over the latter throughout the decay period, as shown in Fig. 5d.

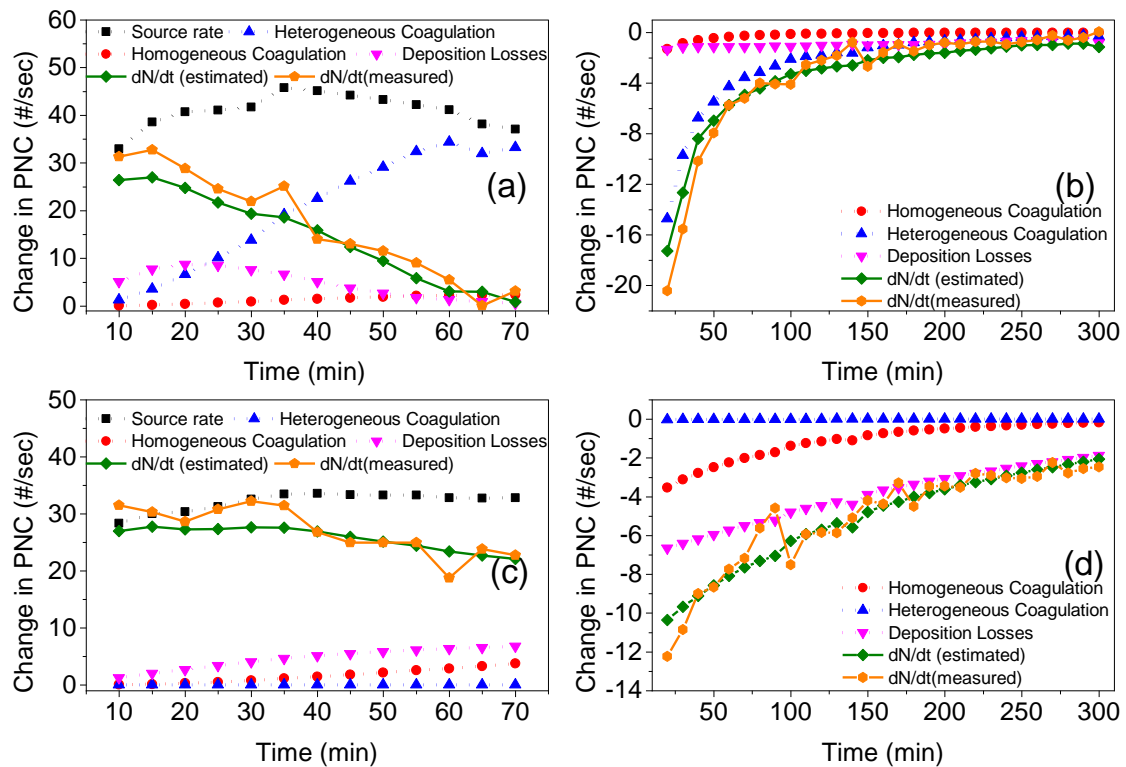


**Fig. 6:** Evolution over time of the average change in PNC (estimated and measured) of SiO<sub>2</sub> aerosol due to coagulation and deposition for (a, b) ultrafine, and (c, d) fine particles during the (a, c) injection stage and the (b, d) 5 h period following the end of injection.

Regarding the SiO<sub>2</sub> dispersion tests, during the early stage of injection, losses of ultrafine particles were dominated by deposition (see Fig. 6a). Contrary to their TiO<sub>2</sub> counterparts, the deposition losses of the SiO<sub>2</sub> ultrafine particles, demonstrated an increasing trend with time, reaching a maximum at the 20<sup>th</sup> minute of injection. Losses due to heterogeneous coagulation also increased during the injection period with an almost linear trend. After this period, as PNC in the chamber increased by the injection of fresh aerosol, heterogeneous coagulation for these particles became dominant and determined their losses up to the end of injection, while deposition losses gradually decreased, reaching almost zero values at the end of the process. Fine particles, similarly to their TiO<sub>2</sub> counterparts, were increasingly removed by deposition throughout the injection process (Fig. 6c), while homogeneous coagulation was also increasing. However, the equivalency between these two removal mechanisms observed in the case of TiO<sub>2</sub> at the end of injection, cannot be seen here.

In the 5 h period following the end of injection, concentrations of SiO<sub>2</sub> ultrafine particles, similar to their TiO<sub>2</sub> counterparts, were governed by losses induced by heterogeneous coagulation (Fig. 6b), while losses due to deposition were low, except for minor contributions estimated at very low PNC, when the relative importance of both coagulation and deposition became almost equal. Fine particles, as can be seen in Figure 6d, were mainly removed by deposition which decreased over time with the decrease of the PNC, while homogeneous coagulation demonstrated a secondary role in the particle removal process throughout this period.

By summing the average results presented above over the specified size groups, then a comparison between the measured and estimated PNC changes, for both materials, for the whole size spectrum of DMS, can be obtained, as shown in Fig. 7. The analytical model is not capable of capturing the fluctuations of PNC that may result for example from localized turbulent flows. However, the temporal changes of total PNC are adequately captured, indicating that an acceptable explanation of the particle mechanisms has been found.

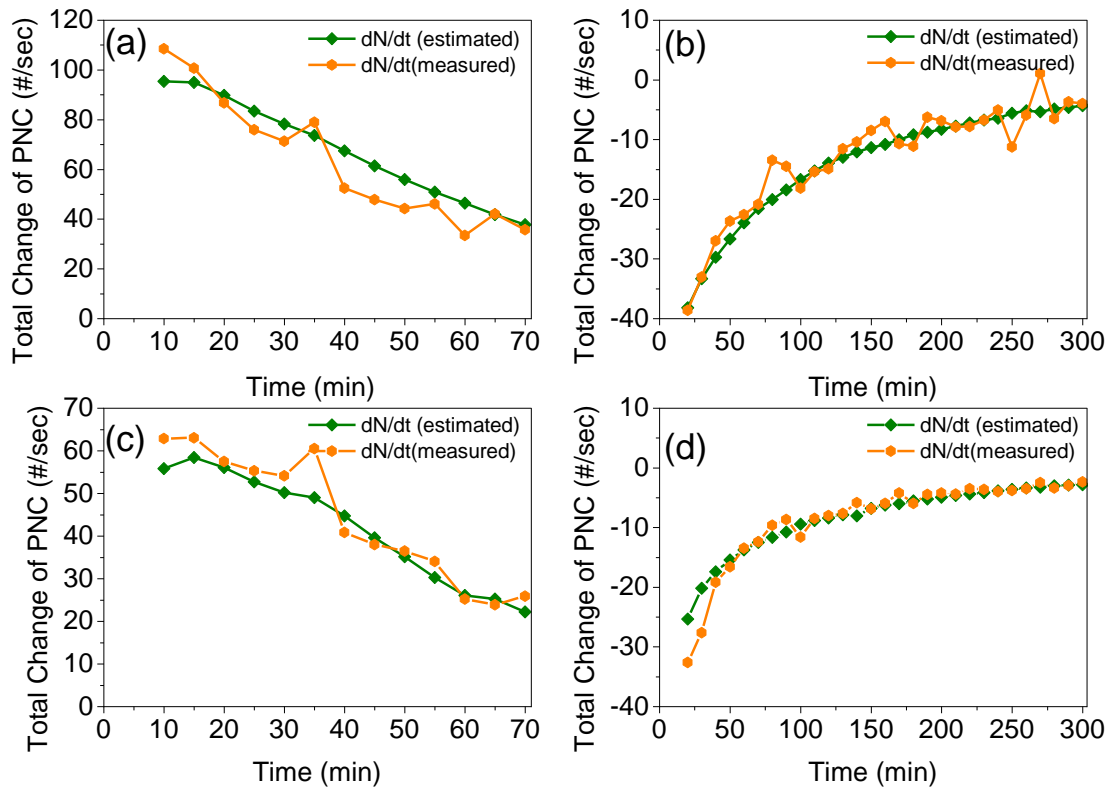


**Fig. 7:** Aggregate model (estimated) and experimental results (measured) of (a, c) the injection stage and (b, d) the 5 hours following the end of injection, for (a, b) TiO<sub>2</sub> and (c, d) SiO<sub>2</sub> respectively. Results refer to the whole size spectrum of the DMS (4.87-1000 nm).

The percentage of loss attributed to coagulation and deposition over time, in ultrafine and fine particles, is shown in Figs. 8 and 9 respectively, for both tested materials. In general, the contribution of deposition in the loss of SiO<sub>2</sub> ultrafine particles over time was substantially higher than that in their TiO<sub>2</sub> counterparts (see Fig. 8), while homogeneous coagulation losses were more intense in the case of the latter than that of the former. On the other hand, during the period of high PNC (end of injection-start of the 5 hour decay period), increased losses due to homogeneous coagulation can be seen for the TiO<sub>2</sub> fine particles compared to their TiO<sub>2</sub> counterparts (Fig. 9). Indicative of that is the 51.5% and 48.5%, and the 35.5% and 64.5%, relative contributions of homogeneous coagulation and deposition to the total particle loss sink over the last 5 min of the injection of TiO<sub>2</sub> and SiO<sub>2</sub>, respectively.

Finally, at the peak particle concentration, irrespective of the material type, the total concentration decay of ultrafine particles was mainly controlled by coagulation (more

than 90% contribution), and as PNC decreased the coagulation related loss decreased with time because a lower concentration results in fewer collisions and lower particle

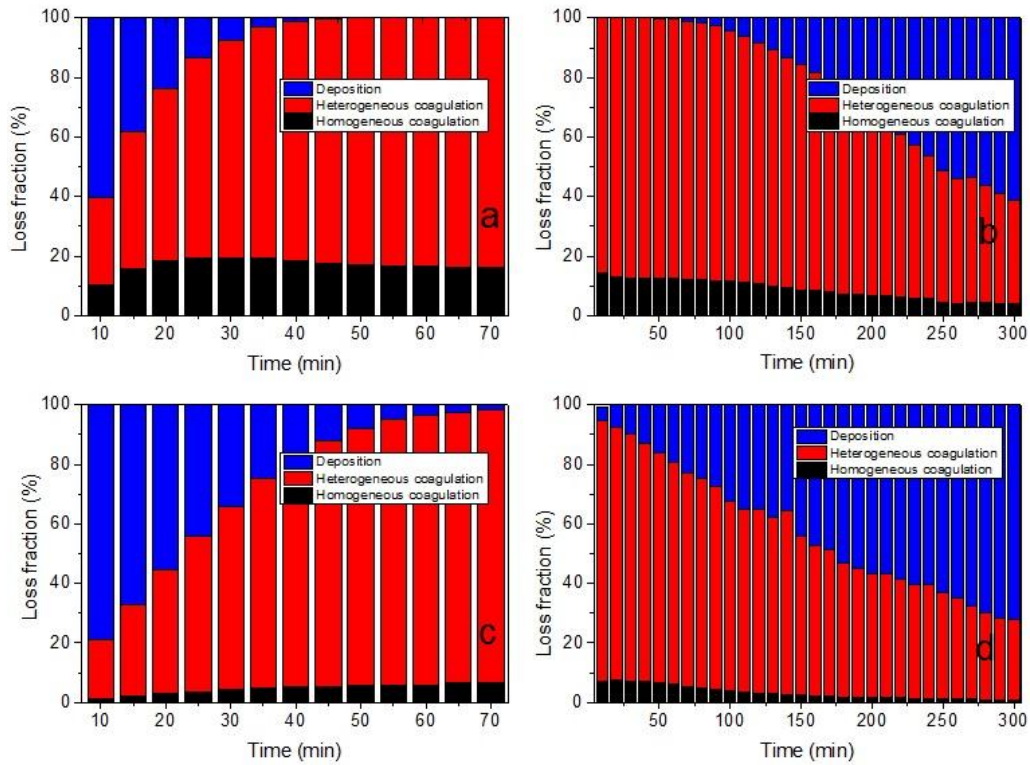


**Fig. 8:** Contribution of coagulation and deposition over time to PNC loss of (a, b) ultrafine TiO<sub>2</sub> particles and (c, d) ultrafine SiO<sub>2</sub> particles, during their (a, c) injection and their (b, d) 5 h decay period.

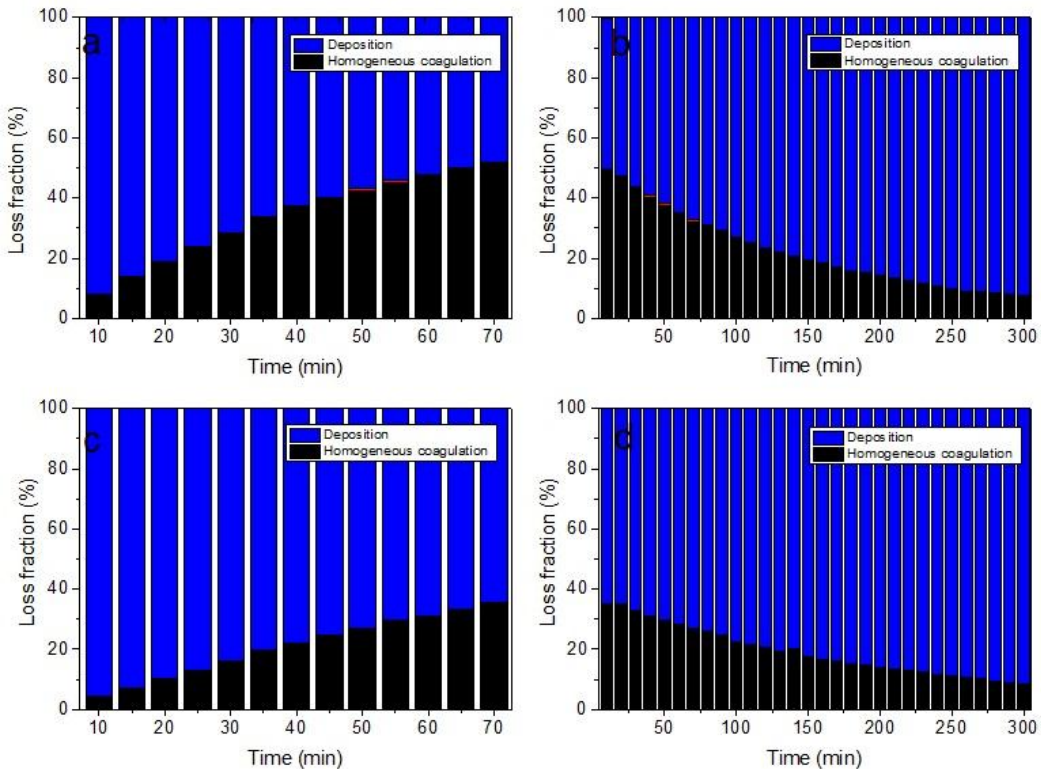


**Fig. 9:** Contribution of coagulation and deposition over time to PNC loss of (a, b) fine TiO<sub>2</sub> particles and (c, d) fine SiO<sub>2</sub> particles, during their (a, c) injection and their (b, d) 5 h decay period.

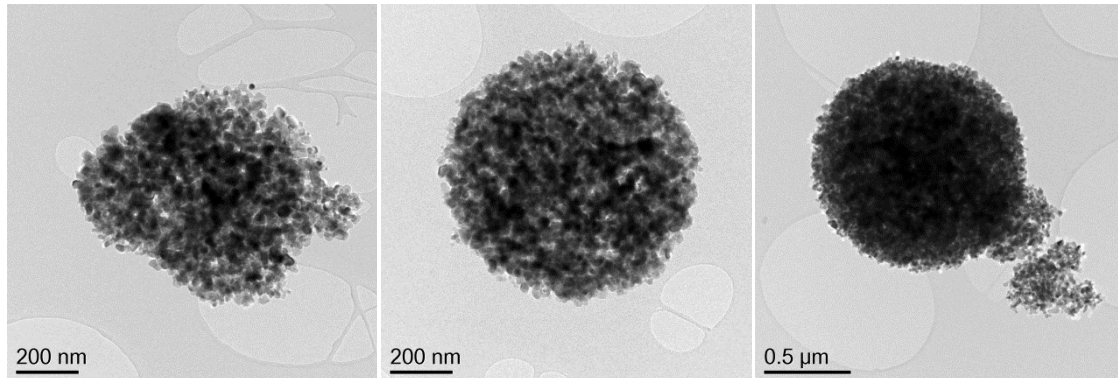
loss rates. At the same time, the amount of deposition significantly increased with time and dominated the concentration decay.

The relative contribution of coagulation and deposition to the decay of indoor polydisperse aerosols, such as aerosolised SiO<sub>2</sub> nanoparticles (Wang et al., 2017), gasoline vehicle exhaust particles (Zhao et al., 2015), and diesel and paper ash particles (Schnell et al., 2006) has been investigated by previous studies, providing the basis for comparisons to the results presented here which correspond to the decay period of the tested aerosols. It should be noted that these studies applied different analytical and computational methods to model coagulation, avoiding the complexity of the pair to pair nanoparticle collision and coagulation theory applied in this work.

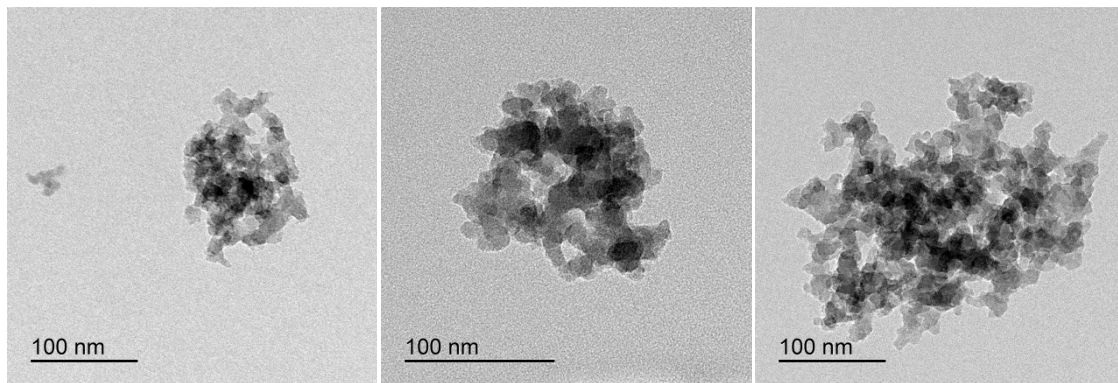
For polydisperse SiO<sub>2</sub> aerosol particles of diameter ranging from 10 to 400 nm, the contribution of the initial coagulation to the total particle loss was of 60%, at an initial peak concentration  $6.0 \times 10^4$  particles cm<sup>-3</sup> (Wang et al., 2017). In the works of Zhao et al. (2015) and Schnell et al. (2006), for particles from gasoline vehicle exhaust of diameter < 100 nm, and for diesel and paper ash particles with initial geometric mean diameter (GMD) 52-227 nm, respectively, it was indicated that during the first 10 min of decay the contribution of coagulation was up to 90% or more (initial peak particle concentration of  $10^5$ - $10^6$  #/cm<sup>-3</sup>). After development of particle decay, the contribution of coagulation decreased with time, while the amount of deposition increased with time, as indicated also in this work.

Complementary information related to the formation and agglomeration characteristics of the deposited particles can be derived from the TEM images shown in Fig. 10. Individual primary particles were not detected on the metal stubs for either of the materials. TiO<sub>2</sub> samples (Fig. 10a) revealed the presence of large spherical shaped formations composed of multiple primary nanoparticles with a relatively high number of detected sizes ranging from some hundreds of nm to more than 1 μm in diameter. Based on the model results, this could be attributed to the strong homogeneous coagulation between fine particles during their airborne phase. In some cases, these large nanoparticle agglomerates were observed to be attached to smaller particles forming chainlike agglomerates, suggesting that the latter were scavenged by

the former undergoing gravitational settling. Similarly, Yu et al. (2013) indicated the role of coagulation in determining the loss of PNC with the increase of total aerosol number concentration.



(a)



(b)

**Fig. 10:** (a) TiO<sub>2</sub> and (b) SiO<sub>2</sub> nanoparticle agglomerates deposited on the floor and the walls of the exposure chamber as captured by TEM.

TEM data also showed a predominance of agglomerated nanoparticles in the SiO<sub>2</sub> samples (Fig. 10b). The average size range of these agglomerates was substantially lower compared to their TiO<sub>2</sub> counterparts, whereas their morphology presented a more rod-shaped structure. Aggregates of small sizes were observed which in some cases reached 50 nm in diameter. The latter is aligned with the strong deposition losses of ultrafine particles, as indicated by the model results for the early stage of SiO<sub>2</sub> injection. Therefore, it is concluded that the deposition patterns obtained by TEM images representing the nanoparticle agglomerates present in the different aerosols, qualitatively support the results obtained with the application of the aerosol dynamic model.

Another interesting aspect derived from the TEM images is that the TiO<sub>2</sub> agglomerates presented a compact structure characterised by a spherical shape within which the primary particles appear to be held together by strong bonds. On the other hand, the SiO<sub>2</sub> agglomerates are shown to consist of primary particles which coalesced to each other with loose bonds. Given that Van der Waal's forces are a determinant factor in the promotion of particle coalescence, and that Hamaker constants in air medium have been estimated to be  $15.3 \times 10^{-20}$  J and  $6.5 \times 10^{-20}$  J (Bergström, 1997), for TiO<sub>2</sub> and SiO<sub>2</sub> particles, respectively, the more strongly bonded structure presented by the TiO<sub>2</sub> deposited agglomerates compared to the SiO<sub>2</sub> ones, seems to be reasonable.

#### **4. Conclusions**

Dispersion experiments were carried out in an enclosed chamber simulating the atmosphere of a workplace, and the variation of size distributions of nanomaterial particles generated from specific nanopowders were measured over a period of time, under stirred conditions and without ventilation.

Novel features of our experiments are: the simultaneous emission and post-emission measurement of PNC via a DMS and an APS which extended the range of the particle size measurements from 0.00487 µm to 20 µm; the integration of experimental observations through the combination of high resolution temporal and size segregated real time sampling, with an off-line analysis (i.e. TEM) of deposited particles; the comparison of experiments with two widely used powdered ENMs, such as TiO<sub>2</sub> and SiO<sub>2</sub>. Furthermore, the combination of analysis of the real time measurements with the development of a particle process model, allowed the relative importance of different particle loss mechanisms (deposition, homogeneous coagulation and heterogeneous coagulation) to be evaluated, for the two particle types.

The evolution of the modal groups presents within the PSDs measured by the DMS was determined through a log<sub>10</sub>-normal fitting program. The study of the time evolution of the modes indicated that the agglomeration effect, in terms of particle growth, is observable after the time required for the chamber's volume to reach sufficiently high PNC under well-mixed conditions to promote particle coagulation. Additionally, it was shown that during the prolonged post injection decay period, the TiO<sub>2</sub> aerosol demonstrated a rapid decrease in PNC within the first hour accompanied

by a relatively stagnant main peak diameter over time, while the SiO<sub>2</sub> aerosol demonstrated a more moderate decrease in PNC accompanied by shifts of the PSD toward larger sizes over time.

Based on a new approach that considers a total particle decay rate incorporating coagulation and deposition losses, the changes in PNC over time caused by the action of these two particle removal mechanisms were accurately modelled using a small number of physical parameters. The modelling results suggested that for ultrafine particles of both tested materials, heterogeneous coagulation was the main particle loss mechanism which increased as the PNC increased within the chamber. In contrast, losses in fine particles were predicted to be mainly dominated by deposition. However, differentiations were observed in the model predictions with respect to the material type. Increased deposition losses of SiO<sub>2</sub> ultrafine particles and increased homogeneous coagulation losses of TiO<sub>2</sub> fine particles, compared to their TiO<sub>2</sub> and SiO<sub>2</sub> counterparts, at low (early injection stage) and high (end of injection-start of the 5 hour decay period) PNC, respectively, were estimated by the model.

The deposition patterns indicated by TEM images representing the nanoparticle agglomerates present in the different aerosols, qualitatively supported the results obtained from the application of the aerosol dynamic model. Furthermore, SiO<sub>2</sub> deposited particles presented more weakly bounded looser structures than their TiO<sub>2</sub> counterparts, and as such may present a greater risk of de-agglomeration under accidental and post-accidental conditions.

Although the application of results presented by this work to real-world situations needs to be carefully performed, as the initial conditions (e.g. the initial PSDs produced by the 6-jet CN, the turbulence intensity induced by the fan, the existence of additional surfaces to those provided by the chamber's wall and floor which may influence the particle deposition rates) may differ significantly to these presented here, this article provides an approximate range of input parameters for mathematical modelling, as well as the means for evaluating the effects of mechanisms governing the indoor behaviour of accidentally released aerosol particles generated from powdered ENMs and their potential risks to human exposure.

## **Acknowledgments**

The authors would like to thank the European Commission 7th Framework program for Research and Technological Development NMP under grant agreement FP7-NMP-2010-LARGE-4, № 263215.

Note: The present paper reflects only the authors' views and the Union is not liable for any use that can be made of the information contained therein.

## **Appendix A**

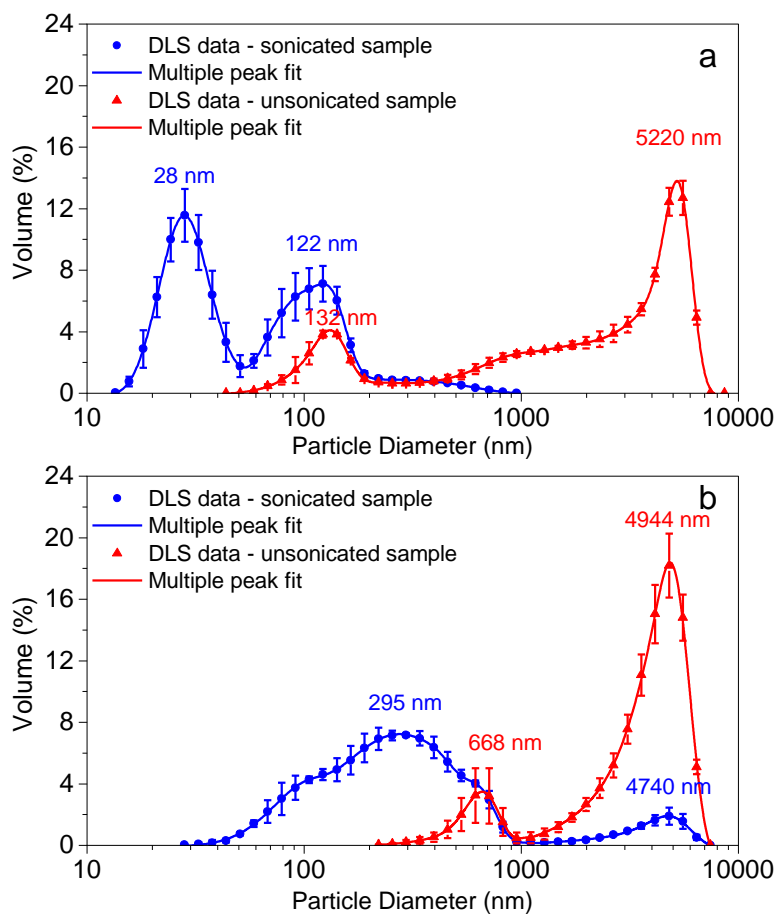


**Fig. A.1:** Volume based average PSD derived by the DLS method of (a) TiO<sub>2</sub> and (b) SiO<sub>2</sub> nanopowders in water suspensions (symbols: experimental data  $\pm 2\sigma$ ; line: multiple peak fit) with and without sonication.

## Appendix B

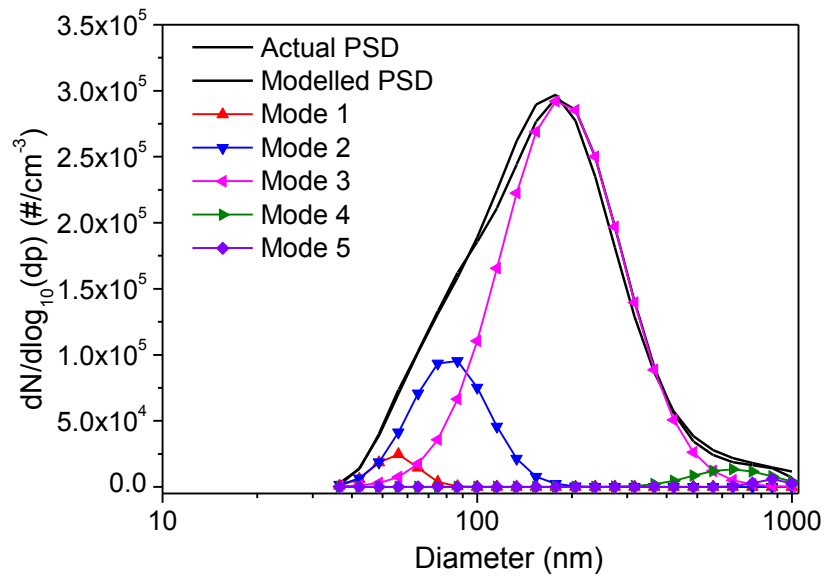


**Fig. B.1:** An averaged PSD of a typical TiO<sub>2</sub> dispersion test, indicating the component log<sub>10</sub>-normal modes fitted by the Rmixdist package

## References

- Agus, E.L., Young, D.T., Lingard, J.J., Smalley, R.J., Tate, J.E., Goodman, P.S., Tomlin, A.S., 2007. Factors influencing particle number concentrations, size distributions and modal parameters at a roof-level and roadside site in Leicester, UK. *Science of the Total Environment* 386, 65-82.
- Asbach, C., Kaminski, H., Lamboy, Y., Schneiderwind, U., Fierz, M., Todea, A.M., 2016. Silicone sampling tubes can cause drastic artifacts in measurements with aerosol instrumentation based on unipolar diffusion charging. *Aerosol Science and Technology* 50, 1375-1384.
- Bergström, L., 1997. Hamaker constants of inorganic materials. *Advances in Colloid and Interface Science* 70, 125-169.
- Blank, F., Gehr, P., Rothen-Rutishauser, B., 2009. In vitro human lung cell culture models to study the toxic potential of nanoparticles. *Nanotoxicity: From in vitro, in vivo models to health risks*, 379-395.
- Brouwer, D.H., Spaan, S., Roff, M., Sleuwenhoek, A., Tuinman, I., Goede, H., van Duuren-Stuurman, B., Filon, F.L., Bello, D., Cherrie, J.W., 2016. Occupational dermal exposure to nanoparticles and nano-enabled products: Part 2, exploration of exposure processes and methods of assessment. *International journal of hygiene and environmental health* 219, 503-512.
- Delmaar, C.J., Peijnenburg, W.J., Oomen, A.G., Chen, J., de Jong, W.H., Sips, A.J., Wang, Z., Park, M.V., 2015. A practical approach to determine dose metrics for nanomaterials. *Environmental Toxicology and Chemistry* 34, 1015-1022.
- Ding, Y., Kuhlbusch, T.A., Van Tongeren, M., Jiménez, A.S., Tuinman, I., Chen, R., Alvarez, I.L., Mikolajczyk, U., Nickel, C., Meyer, J., 2017. Airborne engineered nanomaterials in the workplace—a review of release and worker exposure during nanomaterial production and handling processes. *Journal of hazardous materials* 322, 17-28.
- Filon, F.L., Mauro, M., Adami, G., Bovenzi, M., Crosera, M., 2015. Nanoparticles skin absorption: New aspects for a safety profile evaluation. *Regulatory Toxicology and Pharmacology* 72, 310-322.
- Gardea-Torresdey, J.L., Rico, C.M., White, J.C., 2014. Trophic transfer, transformation, and impact of engineered nanomaterials in terrestrial environments. *Environmental science & technology* 48, 2526-2540.
- Gottschalk, F., Sun, T., Nowack, B., 2013. Environmental concentrations of engineered nanomaterials: review of modeling and analytical studies. *Environmental Pollution* 181, 287-300.
- He, C., Morawska, L., Gilbert, D., 2005. Particle deposition rates in residential houses. *Atmospheric Environment* 39, 3891-3899.
- Hinds, W.C., 1999. *Aerosol Technology: Properties, Behavior, and Measurement of airborne Particles* (2nd edition).
- Hussein, T., Hruška, A., Dohányosová, P., Džumbová, L., Hemerka, J., Kulmala, M., Smolík, J., 2009. Deposition rates on smooth surfaces and coagulation of aerosol particles inside a test chamber. *Atmospheric Environment* 43, 905-914.
- Jamriska, M., Morawska, L., 2003. Quantitative assessment of the effect of surface deposition and coagulation on the dynamics of submicrometer particles indoors. *Aerosol Science & Technology* 37, 425-436.
- John, A.C., Küpper, M., Manders-Groot, A.M., Debray, B., Lacombe, J.-M., Kuhlbusch, T.A., 2017. Emissions and possible environmental implication of engineered nanomaterials (ENMs) in the atmosphere. *Atmosphere* 8, 84.
- Kermanizadeh, A., Gosens, I., MacCalman, L., Johnston, H., Danielsen, P.H., Jacobsen, N.R., Lenz, A.-G., Fernandes, T., Schins, R.P., Cassee, F.R., 2016. A

multilaboratory toxicological assessment of a panel of 10 engineered nanomaterials to human health—ENPRA project—the highlights, limitations, and current and future challenges. *Journal of Toxicology and Environmental Health, Part B* 19, 1-28.

Klaine, S.J., Koelmans, A.A., Horne, N., Carley, S., Handy, R.D., Kapustka, L., Nowack, B., von der Kammer, F., 2012. Paradigms to assess the environmental impact of manufactured nanomaterials. *Environmental Toxicology and Chemistry* 31, 3-14.

Koivisto, A. J., Jensen, A. C. Ø., Kling, K. I., Nørgaard, A., Brinch, A., Christensen, F., & Jensen, K. A. (2017). Quantitative material releases from products and articles containing manufactured nanomaterials: Towards a release library. *NanoImpact*, 5, 119-132.

Kuhlbusch, T.A., Asbach, C., Fissan, H., Göhler, D., Stintz, M., 2011. Nanoparticle exposure at nanotechnology workplaces: a review. *Particle and fibre toxicology* 8, 22.

Kulmala, M., Maso, M., Mäkelä, J., Pirjola, L., Väkevä, M., Aalto, P., Miiikkulainen, P., Hämeri, K., O'dowd, C., 2001. On the formation, growth and composition of nucleation mode particles. *Tellus B* 53, 479-490.

Kylafis, G.F., 2016. The Explosion and Dispersion Potential of Engineered Nanoparticles, PhD thesis. University of Leeds. Available at: <http://etheses.whiterose.ac.uk/15618/>.

Lai, A., Nazaroff, W., 2005. Supermicron particle deposition from turbulent chamber flow onto smooth and rough vertical surfaces. *Atmospheric Environment* 39, 4893-4900.

Lai, A.C., 2002. Particle deposition indoors: a review. *Indoor air* 12, 211-214.

Lai, A.C., 2006. Particle deposition and decay in a chamber and the implications to exposure assessment. *Water, Air, and Soil Pollution* 175, 323-334.

Lai, A.C., Byrne, M.A., Goddard, A.J., 2002. Experimental studies of the effect of rough surfaces and air speed on aerosol deposition in a test chamber. *Aerosol Science & Technology* 36, 973-982.

Leys, J., McTainsh, G., Koen, T., Mooney, B., Strong, C., 2005. Testing a statistical curve-fitting procedure for quantifying sediment populations within multi-modal particle-size distributions. *Earth Surface Processes and Landforms* 30, 579-590.

Lingard, J.J., Agus, E.L., Young, D.T., Andrews, G.E., Tomlin, A.S., 2006. Observations of urban airborne particle number concentrations during rush-hour conditions: analysis of the number based size distributions and modal parameters. *Journal of Environmental Monitoring* 8, 1203-1218.

Maynard, A.D., Kuempel, E.D., 2005. Airborne nanostructured particles and occupational health. *Journal of nanoparticle research* 7, 587-614.

Maynard, A.D., Zimmer, A.T., 2003. Development and validation of a simple numerical model for estimating workplace aerosol size distribution evolution through coagulation, settling, and diffusion. *Aerosol Science & Technology* 37, 804-817.

Methner, M., Hodson, L., Dames, A., Geraci, C., 2010a. Nanoparticle emission assessment technique (NEAT) for the identification and measurement of potential inhalation exposure to engineered nanomaterials—Part B: Results from 12 field studies. *Journal of occupational and environmental hygiene* 7, 163-176.

Methner, M., Hodson, L., Geraci, C., 2010b. Nanoparticle emission assessment technique (NEAT) for the identification and measurement of potential inhalation exposure to engineered nanomaterials—Part A. *Journal of occupational and environmental hygiene* 7, 127-132.

Mönkkönen, P., Koponen, I., Lehtinen, K., Uma, R., Srinivasan, D., Hämeri, K., Kulmala, M., 2004. Death of nucleation and Aitken mode particles: observations at extreme atmospheric conditions and their theoretical explanation. *Journal of aerosol science* 35, 781-787.

Muhlfeld, C., Gehr, P., Rothen-Rutishauser, B., 2008. Translocation and cellular entering mechanisms of nanoparticles in the respiratory tract. *Swiss medical weekly* 138, 387.

Nazarenko, Y., Zhen, H., Han, T., Li, P.J., Mainelis, G., 2012. Potential for inhalation exposure to engineered nanoparticles from nanotechnology-based cosmetic powders. *Environmental health perspectives* 120, 885.

Oberdörster, G., Castranova, V., Asgharian, B., Sayre, P., 2015. Inhalation exposure to carbon nanotubes (CNT) and carbon nanofibers (CNF): Methodology and dosimetry. *Journal of Toxicology and Environmental Health, Part B* 18, 121-212.

Pattan, G., Kaul, G., 2014. Health hazards associated with nanomaterials. *Toxicology and industrial health* 30, 499-519.

Rim, D., Green, M., Wallace, L., Persily, A., Choi, J.-I., 2012. Evolution of ultrafine particle size distributions following indoor episodic releases: relative importance of coagulation, deposition and ventilation. *Aerosol Science and Technology* 46, 494-503.

Schneider, T., Brouwer, D.H., Koponen, I.K., Jensen, K.A., Fransman, W., Van Duuren-Stuurman, B., Van Tongeren, M., Tielemans, E., 2011. Conceptual model for assessment of inhalation exposure to manufactured nanoparticles. *Journal of Exposure Science and Environmental Epidemiology* 21, 450-463.

Schnell, M., Cheung, C., Leung, C., 2006. Investigation on the coagulation and deposition of combustion particles in an enclosed chamber with and without stirring. *Journal of aerosol science* 37, 1581-1595.

Seipenbusch, M., Binder, A., Kasper, G., 2008. Temporal evolution of nanoparticle aerosols in workplace exposure. *Annals of occupational hygiene* 52, 707-716.

Thatcher, T.L., Lai, A.C., Moreno-Jackson, R., Sextro, R.G., Nazaroff, W.W., 2002. Effects of room furnishings and air speed on particle deposition rates indoors. *Atmospheric environment* 36, 1811-1819.

Von der Weiden, S., Drewnick, F., Borrmann, S., 2009. Particle Loss Calculator—a new software tool for the assessment of the performance of aerosol inlet systems. *Atmos. Meas. Tech* 2, 479-494.

Wallace, L., Wang, F., Howard-Reed, C., Persily, A., 2008. Contribution of gas and electric stoves to residential ultrafine particle concentrations between 2 and 64 nm: size distributions and emission and coagulation rates. *Environmental Science & Technology* 42, 8641-8647.

Wallace, L.A., Emmerich, S.J., Howard-Reed, C., 2004. Source strengths of ultrafine and fine particles due to cooking with a gas stove. *Environmental Science & Technology* 38, 2304-2311.

Walser, T., Hellweg, S., Juraske, R., Luechinger, N.A., Wang, J., Fierz, M., 2012. Exposure to engineered nanoparticles: model and measurements for accident situations in laboratories. *Science of the Total Environment* 420, 119-126.

Wang, Y., Chen, L., Chen, R., Tian, G., Li, D., Chen, C., Ge, X., Ge, G., 2017. Effect of relative humidity on the deposition and coagulation of aerosolized SiO<sub>2</sub> nanoparticles. *Atmospheric Research* 194, 100-108.

Whitby, K.T., 1978. The physical characteristics of sulfur aerosols. *Atmospheric Environment (1967)* 12, 135-159.

Yu, M., Koivisto, A.J., Hämeri, K., Seipenbusch, M., 2013. Size dependence of the ratio of aerosol coagulation to deposition rates for indoor aerosols. *Aerosol Science and Technology* 47, 427-434.

Zhao, Y., Wang, F., Zhao, J., 2015. Size-resolved ultrafine particle deposition and Brownian coagulation from gasoline vehicle exhaust in an environmental test chamber. *Environmental science & technology* 49, 12153-12160.

### **Highlights**

- Size resolved particle dispersion experiments with engineered nanomaterials in an enclosed chamber simulating the atmosphere of a workplace;
- Quantification of coagulation and deposition through the application of a particle process model;
- The changes in size-resolved PNC over time were accurately modelled using a small number of physical parameters;
- The particle deposition patterns illustrated by TEM images qualitatively supported the model results.